

# LOAN DOCUMENT

PHOTOGRAPH THIS SHEET

①

INVENTORY

AD-A263 483



DTIC ACCESSION NUMBER

LEVEL

WL-TR-93-2060

DOCUMENT IDENTIFICATION

Oct 92

## DISTRIBUTION STATEMENT A

Approved for public release  
Distribution Unlimited

DISTRIBUTION STATEMENT

### ACCESSION FOR

NTIS ☒ GRAB  
DTIC ☐ TRAC  
UNANNOUNCED  
JUSTIFICATION

BY

DISTRIBUTION/

AVAILABILITY CODES

DISTRIBUTION

AVAILABILITY AND/OR SPECIAL

A-1

DISTRIBUTION STAMP

DTIC STAMP

DTIC  
ELECTE  
APR 23 1993  
S C D

DATE ACCESSIONED

DATE RETURNED

93 1 10 17

DATE RECEIVED IN DTIC

93-08332



3928

REGISTERED OR CERTIFIED NUMBER

PHOTOGRAPH THIS SHEET AND RETURN TO DTIC-FDAC

H  
A  
N  
D  
L  
E  
  
W  
I  
T  
H  
  
C  
A  
R  
E

WL-TR-93-2060

IMPROVED HEAT REMOVAL BY MICROSCOPIC  
SURFACE TEXTURING OF CAPILLARIES



DR. CHARLES C BLATCHLEY

SPIRE CORPORATION  
ONE PATRIOTS PARK  
BEDFORD MA 01730-2396

OCTOBER 1992

FINAL REPORT FOR 04/01/92-10/30/92

APPROVED FOR PUBLIC RELEASE; DISTRIBUTION IS UNLIMITED.

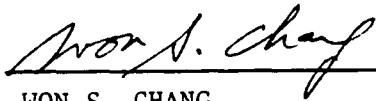
AEROPROPULSION AND POWER DIRECTORATE  
WRIGHT LABORATORY  
AIR FORCE MATERIEL COMMAND  
WRIGHT PATTERSON AFB OH 45433-7650

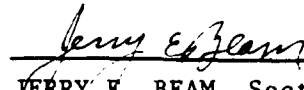
## NOTICE


When Government drawings, specifications, or other data are used for any purpose other than in connection with a definitely Government-related procurement, the United States Government incurs no responsibility or any obligation whatsoever. The fact that the government may have formulated or in any way supplied the said drawings, specifications, or other data, is not to be regarded by implication, or otherwise in any manner construed, as licensing the holder, or any other person or corporation; or as conveying any rights or permission to manufacture, use, or sell any patented invention that may in any way be related thereto.

This report is releasable to the National Technical Information Service (NTIS). At NTIS, it will be available to the general public, including foreign nations.

This technical report has been reviewed and is approved for publication.

  
WON S. CHANG  
Project Engineer

  
JERRY E. BEAM, Section Chief  
Power Technology Branch  
Aerospace Power Division  
Aero Propulsion and Power Directorate

  
MICHAEL D. BRAYDICH, Lt Col, USAF  
Deputy Chief  
Aerospace Power Division  
Aero Propulsion & Power Directorate

If your address has changed, if you wish to be removed from our mailing list, or if the addressee is no longer employed by your organization please notify WL/POOS, WPAFB, OH 45433-7650 to help us maintain a current mailing list.

Copies of this report should not be returned unless return is required by security considerations, contractual obligations, or notice on a specific document.

OCT 1992 FINAL  
IMPROVED HEAT REMOVAL BY MICROSCOPIC  
SURFACE TEXTURING OF CAPILLARIES

04/01/92--10/30/92

C F33615-92-C-2252

PE 63218

PR 1602

TA 01

WU 02

DR. CHARLES C BLATCHLEY

SPIRE CORPORATION  
ONE PATRIOTS PARK  
BEDFORD MA 01730-2396

AEROPROPULSION AND POWER DIRECTORATE  
WRIGHT LABORATORY  
AIR FORCE MATERIEL COMMAND  
WRIGHT PATTERSON AFB OH 45433-7650

WL-TR-93-2060

THIS IS A SMALL BUSINESS INNOVATIVE RESEARCH PROGRAM,  
PHASE I REPORT.

APPROVED FOR PUBLIC RELEASE; DISTRIBUTION IS  
UNLIMITED.

Phase I demonstrated that ion beam microtexturing of metal surfaces enhances heat transfer under three conditions: 1) thermal radiation emission at relatively high temperatures, 2) forced convection, and 3) nucleate boiling. Features were too small to significantly affect heat transfer under non-flowing constant phase conditions. For nucleate boiling, combining microtexture with large scale structures, and after optimizing the texturing process, it should be possible to achieve a composite enhancement better than 20 times the nucleate-boiling heat transfer from a smooth surface. Ion texturing processes produce rugged broad-band light absorbers, completely black from the visible to long wavelength IR. At higher temperature ranges, enhanced radiation adds significantly to total heat transferred. Thus, heat pipes, capillaries, and higher temperature radiators would all perform better with microtextured surfaces.

TEXTURING, HEAT REJECTION, ION BEAMS, ACTIVE  
COOLING, PROPULSION, NUCLEATE BOILING, EMISSIVITY,  
BLACKBODY

38

UNCLASSIFIED

UNCLASSIFIED

UNCLASSIFIED

UL



## TABLE OF CONTENTS

		<u>Page</u>
1	EXECUTIVE SUMMARY .....	1
	1.1 Description of Results .....	1
	1.2 Summary of Conclusions and Recommendations .....	2
	1.3 Contract Statement of Work .....	2
2	TECHNICAL BACKGROUND .....	3
	2.1 Ion Beam Texturing .....	3
	2.2 How Micro-texture Can Approximate Blackbody Emissivity .....	4
	2.3 How Ion Beams Form Micro-Texture .....	12
	2.4 Application to Heat Transfer .....	14
3	EXPERIMENTAL PROCEDURE .....	17
4	RESULTS .....	20
5	CONCLUSIONS AND RECOMMENDATIONS .....	28
	5.1 Conclusions .....	28
	5.2 Recommendations .....	28
6	REFERENCES .....	30

## LIST OF ILLUSTRATIONS

		<u>Page</u>
1	Representative ion beam texturing results: (a) in aluminum using a tantalum seed and (b) in copper .....	3
2	Schemes for seeding to produce microscopic texture by ion beam bombardment ..	4
3	Micro-texturing falls neatly between long wavelength (a) and short wavelength (b) conditions, so neither set of approximations works very well .....	5
4	Reflectance at normal incidence from a surface with a dual distribution of features, from reference 19 .....	6
5	Shadowing functions (multiplier) calculated by various authors (1965-69) for two ratios of rms height to correlation length .....	11
6	Microtexture is caused by differential sputtering between substrate and protective islands formed by seed material agglomerating on the surface .....	12
7	Sigmund model prediction of sputtering rate as a function of incidence angle for 1 keV argon ions bombarding aluminum .....	14
8	Typical space radiator application (SP 100 concept from reference 52) .....	15
9	Effect of surface wettability on bubble contact angle .....	15
10	Ion beam texturing facility .....	17
11	Plasma immersion texturing in an Electron Cyclotron Resonance (ECR) chamber .....	18
12	Calorimeter scheme for fluid transfer tests .....	19
13	1,000X and 5,000X SEM micrographs of ion beam textured copper disk produced by six hours of argon bombardment at 1 keV through a tantalum mesh at a temperature of 450°F .....	20
14	2,000X and 5,000X SEM micrographs of ion beam textured aluminum disk produced by four hours of argon bombardment at 1 keV through a tantalum mesh at a temperature of 480°F .....	21
15	BRDF for textured copper disk .....	22
16	FTIR reflectivity for textured copper disk .....	22

## LIST OF ILLUSTRATIONS (Concluded)

		<u>Page</u>
17	BRDF for three textured aluminum disks .....	23
18	FTIR reflectivity for textured aluminum disk .....	23
19	Representative values of total, normal emissivity .....	24
20	Pool boiling experiment comparing ion beam textured copper with bare metal and natural convection .....	25
21	Pool boiling experiment comparing Turbo-B and two versions of High Flux structure in copper with bare metal and natural convection .....	26
22	Schematic drawings of commercially available structures advertised to enhance the heat transfer coefficient during nucleate boiling by up to a factor of 10 .....	26

## LIST OF TABLES

		<u>Page</u>
I	Effect of ion implantation and texture on selected materials .....	24
II	Average time to change one liter of water from 20 to 25°C through a 40 mm diameter metal sample held at 80°C, in minutes with three trials for each condition .....	27



## SECTION 1 EXECUTIVE SUMMARY

### 1.1 Description of Results

Phase I testing successfully demonstrated that ion beam microtexturing of metal surfaces enhances heat transfer in three general configurations: (1) pure thermal emission, (2) forced convection to non-boiling fluids, and (3) nucleate boiling. The first one requires relatively high temperatures for the texture enhancement to be effective. Convection and nucleate boiling, however, can work at much lower temperatures using refrigerant fluids with low boiling points.

Eight aluminum and five copper disks were separately textured using a 1 keV Argon beam directed through a tantalum mesh to seed differential sputtering. Resulting feature sizes were 0.1 to 1  $\mu\text{m}$  producing diffuse gray to black surfaces. These disks were then used in a simple calorimeter jig to compare heating rates with the corresponding bare metals in contact with flowing and stationary water. Emissivity was evaluated using FTIR spectrometry in air. Lambertian scattering characteristics were demonstrated by measuring the Bidirectional Reflectance Distribution Function (BRDF) in the visible (0.633  $\mu\text{m}$ ) and the IR (10.6  $\mu\text{m}$ ).

Heat transfer by conductivity to a static non-boiling fluid was not significantly enhanced at low temperatures, but moving fluid (convective) heat transfer was. Thermal emittance of the textured surfaces is typically greater than 0.95, which could contribute to heat transfer at moderately high temperatures. For a purely radiative design, this could easily result in a factor of four or five improvement in heat loss over bare metal, since textured surfaces often approximate an ideal blackbody. Emissivity is strongly enhanced over a broad range that can be adjusted to adapt to different operating requirements. Application to radiator fins is possible now without further refinement.

In separate tests, nucleate boiling enhancement was measured at the Rensselaer Polytechnic Institute's Department of Mechanical Engineering by Professor Michael K. Jensen. For these tests, Spire ion-beam textured the outside of a copper cylinder containing a built-in heater element. Texture was produced by immersion in an electron cyclotron resonance (ECR) plasma at an argon pressure of  $4 \times 10^{-5}$  torr. A cylindrical tantalum mesh surrounded the copper element, and both were biased to -1,000 V to extract argon ions from the plasma. The resulting texture was not completely uniform due to seams and thermal distortion of the tantalum mesh, but this can be easily corrected.

Based on the average heat transfer coefficient for the entire cylinder, the maximum improvement in the treated areas was estimated to be about 50%. However, nucleation began at a much lower heat flux in the darkly textured zones, nearly a factor of four below that of the smooth material. At lower heat fluxes, nucleation was observed only in the textured parts. Low flux nucleation may be the single most important enhancement for heat pipes.

## 1.2 Summary of Conclusions and Recommendations

Immediate application of microtexturing to thermal emission applications is warranted with simple tuning of feature size to match the desired emission band. Applications to nucleate boiling and forced convective transfer are also feasible, but additional testing and optimization of surface morphology is likely to improve performance. Hybrid systems of microtexture and larger structures are most likely to yield the highest heat transfers, so these should be developed concurrently with improvements of microtexture performance.

## 1.3 Contract Statement of Work

The following summarizes major tasks completed under this contract:

Task 1 - Generating Artificial Surface Texture

Task 2 - Measure Heat Transfer Per Unit Area

Task 3 - Reporting

## SECTION 2 TECHNICAL BACKGROUND

### 2.1 Ion Beam Texturing

Ion beam texturing was first described in 1942, before it could be imaged by electron microscopy, based on angular changes in reflectivity of glow-discharge cathodes.<sup>1</sup> Since then, many researchers have studied the ion texturing processes and the physical mechanisms involved have become relatively clear.<sup>2</sup> Many of the early investigations were completed at NASA's Lewis Research Center.<sup>3,4</sup> Newer texturing applications have focussed on optical properties. Typical results are shown in Figure 1.

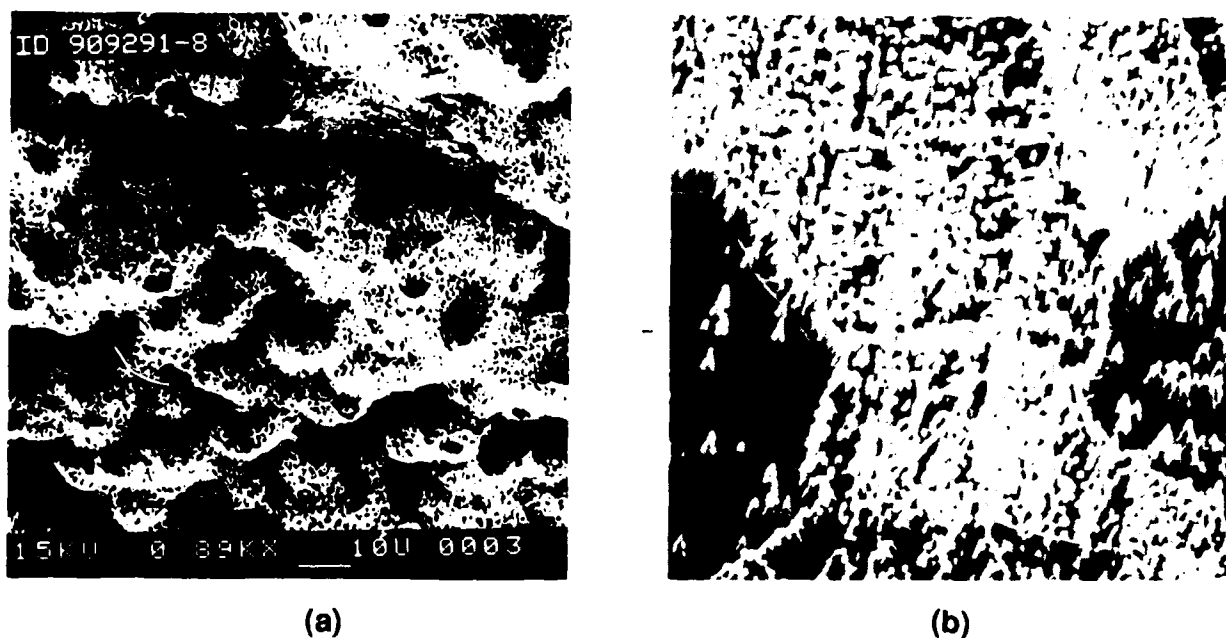


**Figure 1** *Representative ion beam texturing results: (a) in aluminum using a tantalum seed and (b) in copper.*

Energetic (keV) ions striking a solid surface collide with target atoms and transfer enough kinetic energy to break atomic bonds in the outer surface layers so that surface atoms are sputtered away. Efficiency of the sputtering process depends mostly on kinematic factors, specifically mass and energy of projectile ions and mass of target atoms. Typically, heavier projectile ions sputter more efficiently, and lighter target atoms are removed more easily than heavy atoms. However, target atoms which form strong chemical bonds to their nearest neighbor atoms are more difficult to remove. For each projectile ion/target atom combination, there is an optimum sputtering energy related to the relative speed of the ion and of binding electrons in the solid.

Components of mixed target materials usually sputter at different rates, as do impurities. If sputtering removes an impurity more slowly, islands of this species may shield the underlying target material from sputter erosion and produce microscopic pillars on the resulting surface. This natural texture has been observed in many classes of materials: metals, ceramics, and polymers.<sup>5</sup> Similarly, artificially deposited "seed" impurities can enhance this texture. If impurities are not randomly deposited but deliberately placed in regular patterns, this effect may intensify for surface texture lithography.<sup>6</sup> Figure 2 illustrates these techniques for introducing micro-texture.

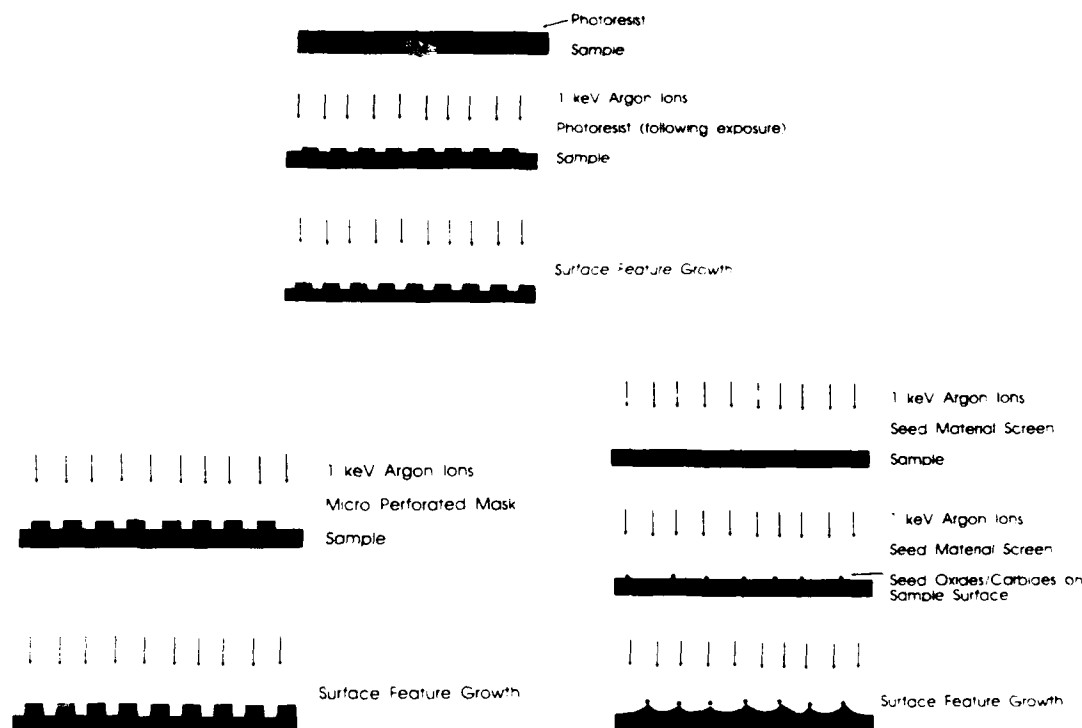


**Figure 2** *Schemes for seeding to produce microscopic texture by ion beam bombardment.*

Other researchers have reported that, for natural texturing, surface temperature governs the size of the texture features formed, apparently through diffusion of impurities away from islands.<sup>7</sup> We have experimentally confirmed this effect and a similar temperature effect for different impurity seed atoms. Residual gasses in the vacuum chamber during ion bombardment also appear to strongly affect feature size.<sup>8</sup>

## 2.2 How Micro-texture Can Approximate Blackbody Emissivity

Spire's development of ion beam micro-textured metals over three years ago was initially directed toward optical baffle materials for suppressing stray light in telescopes. Depending on the exact surface morphology, textured metals have an unexpectedly broad absorption band. When used to shield optical trains in telescopes, they help in viewing or tracking of dim light sources near the sun or other bright source. Since even the darkest materials still reflect at oblique angles, the most effective configurations use these black surfaces to create baffles along the boundaries of the desired viewing rays.

Broadband absorption also makes these materials efficient thermal emitters through Kirchoff's law for opaque surfaces (conservation of energy). Reflectivity and emissivity must add to 100%. Thus, if their unexpected absorption can be explained, so can their emissivity.

Possible explanations include light trapping, diffractive multiple scattering, and shadowing, but these have yet to account for all of the absorption (emission) enhancement. One possibility is that micro-texture uniquely enables multiple scattering to create the conditions needed for photonic localization, an analogue of electron localization in semiconductors, leading to a photonic bandgap.

Multiple scattering from optical surfaces was first treated for scalar waves and a number of types of microscopic surface features by theorists in the 1950s<sup>9-11</sup> with later vectorial treatment<sup>12</sup> and several applications to surfaces similar to those of micro-textured metals since then.<sup>13,14</sup> The full vectorial representation is needed to accurately describe the coupled fields of electromagnetic waves and polarization effects.

Most simplified theories of light scattering are based on either long or short wavelength approximations, relative to the size of scatterers as shown in Figure 3. Neither assumption applies in this case. Statistical techniques, based on distributions of feature sizes, were first worked out for photon scattering from special types of surfaces<sup>15,16</sup> and for radar scattering from ocean waves.<sup>17</sup> These led to first a long wavelength treatment for photons<sup>18</sup> and finally a general statistical treatment.<sup>19</sup>

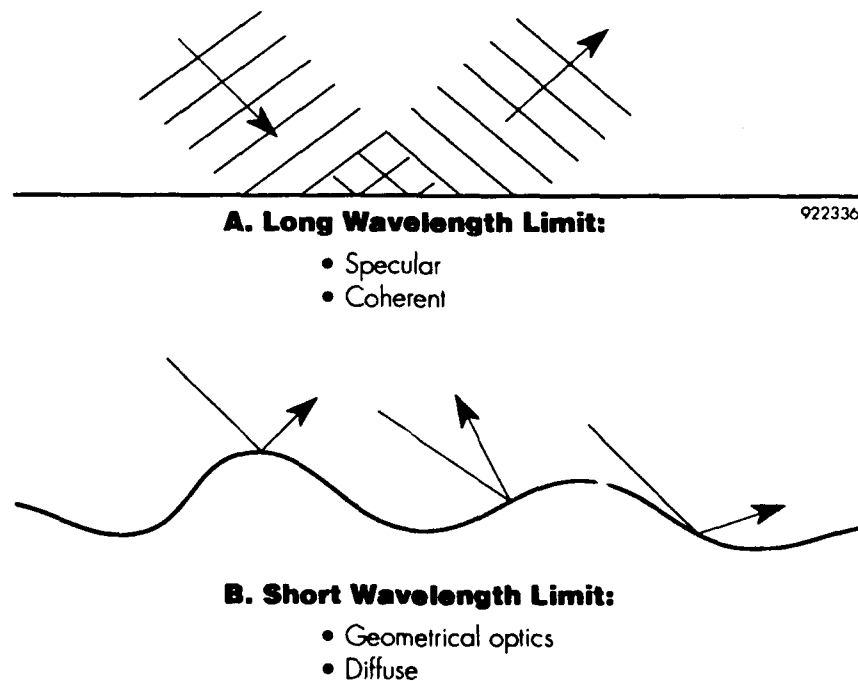


**Figure 3** *Micro-texturing falls neatly between long wavelength (a) and short wavelength (b) conditions, so neither set of approximations works very well.*

The same formalism also applies directly to acoustics,<sup>20</sup> electrons moving through solids,<sup>21</sup> and other wave scattering phenomena, including particles interacting with atomic nuclei.<sup>22</sup> These connections for scattering theory are significant, because the hypothesized related phenomenon of localization was first developed by Anderson for electrons in semiconductors.<sup>23</sup> It has similarly been derived for photon<sup>24-28</sup> and sound scattering,<sup>29-31</sup> but it has been difficult to demonstrate due to the complexity of other interactions.

For general statistical treatments, surface roughness can be characterized by parameters of a Gaussian distribution of random surface heights, namely, average height (rms roughness), and standard deviation. The assumption of randomness ignores individual feature shapes, but it allows straightforward mathematical characterization of the surface through the autocorrelation function, a common basis for Fourier transforms.

Distributions with clusters about more than one mean (effectively superposition of multiple Gaussian distributions) result in very different minima due to interference, but in general, the statistical derivation produces two terms, one for coherent scattering that dominates for long wavelengths where diffraction is important, and one for incoherent scattering that dominates for shorter wavelengths that can be treated by geometrical optics.

Both terms typically go to zero near wavelengths about  $2\pi$  times the average feature size, as shown in Figure 4, but overlap between the terms and other effects prevent the total scattering from vanishing at any one point. Inclusion of multiple scattering<sup>32</sup> generally fills in minima in the total or creates highly localized minima. The fact that micro-textured metals create a relatively broad wavelength region with nearly complete absorption implies that other processes besides scattering are involved.

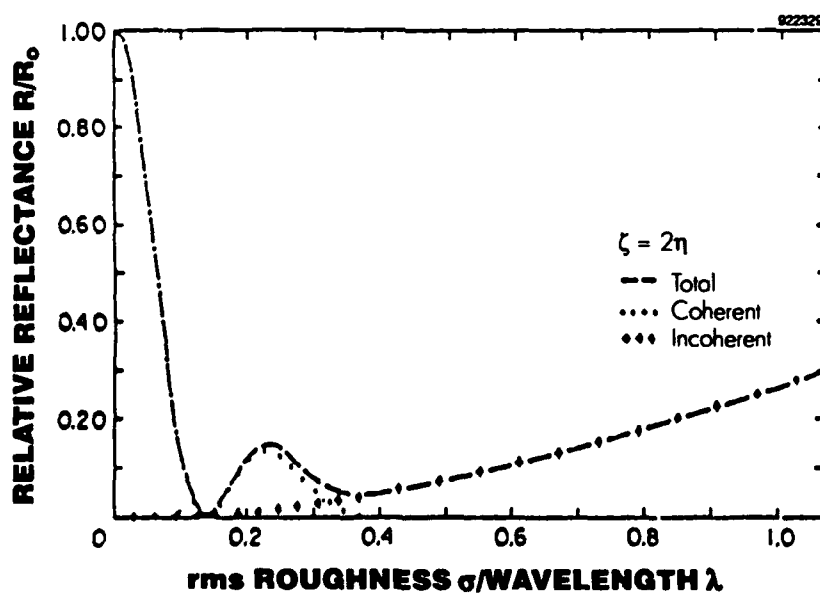


Figure 4 Reflectance at normal incidence from a surface with a dual distribution of features, from reference 19.

Since the feature sizes produced by ion beam texturing are in the range that is most difficult to analyze by non-statistical methods for the wavelengths of interest, it was assumed that the broad absorption observed must be due to the minor differences between theoretical features (typically hemispheres or cylindrical corrugations) and the actual surface configuration. Similar reasoning was used to explain the exceptional darkness of metal blacks, such as goldblack.<sup>33,34</sup>

In photon localization, scattering centers and the spaces between them trap incident photons in standing waves until they are absorbed. The process is exactly analogous to the trapping of electrons in semiconductors resulting in an effective photonic band gap. The difference between localization and ordinary multiple scattering is that multiple scattering presumably stops after a relatively small number of scattering events. Localization implies that a trapped photon scatters indefinitely until absorbed.

Another category of possible explanations is that of simply enhancing absorption in combination with multiple scattering. For example, anodization blackening often includes pigment added to enhance darkening due to texture. Another possibility is that electric permittivity and magnetic permeability of the base metal and oxide coating create absorption over a broad range of wavelengths. Such structures have been deliberately engineered to absorb microwave and longer wavelengths for cooking ware in microwave ovens.

One difficulty in modeling the process has been in the construction of an appropriate auto-correlation function for the unique morphology produced by ion beam texturing, or by chemical etching for that matter, which is definitely non-random and non-Gaussian. The key difference is that the cones and cavities in textured surfaces strongly shadow one another, and these shadows are strongly affected by diffraction because of the size of the features casting them.

Theoretical models have been found which treat both fractal effects and self-shadowing, although they do exclude re-entrant or undercut cavities. Key predictions are that (1) extra darkening (beyond Kirchhoff/Gaussian models) is less significant closer to normal angles of incidence, and (2) that polarization (depolarization) effects are strongly angle dependent due to multiple scattering.

These models are based on the assumptions that textured metals have (1) randomly rough surfaces, that (2) were well-approximated by a Gaussian distribution:

$$p(h) = \frac{1}{\sigma\sqrt{2\pi}} \exp\left(-\frac{h^2}{2\sigma^2}\right) \quad (1)$$

where  $p(h)$  is the probability of finding a particular height  $h$  above an average or base height of zero, and  $\sigma$  is the standard deviation for which 96% of the feature heights are within  $\pm 2\sigma$  of the mean (zero). For this highly symmetric case,  $\sigma$  is the same as the root-mean-square (rms) surface height.

Established scattering theory predicts that this type of surface has a relatively narrow absorption band (one decade) between the zones of coherent and incoherent scattering roughly centered at the wavelength  $\lambda = 2\pi\sigma$ . This is true even for the case of superposition of two Gaussian distributions (shown above in Figure 3) with different rms values showing a broader absorption band with two minima, one for each value of  $2\pi\sigma$ .<sup>19</sup> However, the broadening is still insufficient to account for our measured absorption.

One problem with these simple scattering models is that ion textured metals are usually far from Gaussian, as is typical of many engineered surfaces.<sup>35,36</sup> Exceptions are surfaces produced by a large number of accumulated localized events. These tend to be near-Gaussian; bead blasting is a good example. In contrast, abrasion tends to preferentially remove positive heights (asperities) while preserving negative ones (pits). The resulting asymmetry produces a highly skewed distribution.

A further definition of a random rough surface is provided by the correlation (or autocorrelation) function defined by integration over an infinite surface (or in the limit of large mean surface area,  $A_M$ ):

$$C(R) = \frac{\langle h(r)h(r+R) \rangle}{\sigma^2} = \lim_{A_M \rightarrow \infty} \frac{1}{A_M \sigma^2} \int_{-\infty}^{+\infty} h(r)h(r+R)dr. \quad (2)$$

Without the normalizing factor  $1/\sigma^2$ , the integral is called an autocovariance function. Regardless of the terminology, the important properties for this function are that it is equal to 1 (or  $1/\sigma^2$  for the autocovariance version) at the origin, and it generally decays to zero as  $R$  increases.

The rate of this decay defines a correlation length which effectively specifies the distance required for points to become uncorrelated. Thus, truly random rough surfaces will show a monotonic Gaussian decay curve:

$$C(R) = \exp\left(-\frac{R^2}{\lambda_o^2}\right) \quad (3)$$

where  $\lambda_o$  is the correlation length and the displacement vector  $R$  has become a scalar for isotropic surfaces. Correlation functions for periodic surfaces, which remain correlated over large distances, do not decay this way. For example, the correlation function for a sinusoidal surface is a cosine function.

Actual surfaces typically fall in between, with short range correlations manifesting as oscillations but with a gradual transition to an exponential type decay. In fact, a correlation function that is often used for its improved fit to data is an exponential:<sup>37-39</sup>

$$C(R) = \exp\left(-\frac{|R|}{\lambda_o}\right) \quad (4)$$

where  $\lambda_o$  again is called a correlation length. The problem with this curve is the discontinuity in its gradient at the origin which interferes with considerations of higher order correlations based on surface gradients and derivatives.

The Fourier transform of the correlation function is the power spectral density function or power spectrum. Using the un-normalized form (autocovariance) produces:

$$P(k) = \frac{\sigma^2}{(2\pi)^2} \int_{-\infty}^{+\infty} C(R)e^{ik \cdot R} dR \quad (5)$$

which can be averaged over the area of the mean surface  $A_M$  as:



$$P(k) = \lim_{A_M \rightarrow \infty} \frac{1}{A_M (2\pi)^2} \left| \int_{-\infty}^{\infty} h(r) e^{ikr} dr \right|^2 \quad (6)$$

As in the correlation function itself, the power spectrum is limited by the finite size of any real sample. This creates an upper wavelength cutoff that may add spurious oscillations.

The distinct value of the power spectrum for characterizing surfaces is that it incorporates information about both the spread of the height distribution about the mean level and variation over the surface. Thus, calculations of scattering are often expressed in terms incorporating the power spectrum. It is typically expressed explicitly in terms of correlation lengths, and total area under the power spectrum gives the variance or power of the surface:

$$\int_{-\infty}^{\infty} P(k) dk = \sigma^2 \quad (7)$$

Principles of physical optics or tangent plane theory were first developed over 100 years ago in Kirchhoff's studies of light diffraction by an aperture, for which a scattered field intensity is derived from the incident field at points along the aperture.<sup>40</sup> The fields are approximated as a superposition of plane waves arriving at an imaginary infinite plane tangent to the real surface. Kirchhoff theory is therefore exact only for a perfectly smooth infinite surface. For textured metal surfaces, this approximation is far from perfect, but it is still a better starting model than perturbation theories that are only valid for very nearly smooth surfaces.

In the Kirchhoff and later physical optics formalism, the fields at the scattering surface are combined with a Green's function appropriate for plane wave propagation into an integral equation. Application of boundary conditions then determines solutions for total scattering or in particular directions, for example, at the specular angle. A perfectly reflecting electrical conductor produces Neuman boundary conditions, while anything else results in Dirichlet conditions.

The Kirchhoff approximation used to define the waves in the integral equation for a scalar field may be simply summarized by:

$$\psi_{Total}(r_o) = [1 + R(r_o)] \psi(r_o) \quad (8)$$

where R is the reflection coefficient (R=1 for Neumann conditions), and the incident field is a monochromatic plane wave:

$$\psi(r) = e^{ikr} \quad (9)$$

For a Gaussian surface, this approximation allows a relatively simple integration, especially for scalar waves. The coherent scattering solution is the same as that from a smooth surface multiplied by an exponential factor:

$$\langle \psi^* \rangle = \psi_o^* e^{-g/2} \quad (10)$$

where  $g = k^2 \sigma^2 (\cos \theta_1 + \cos \theta_2)^2$ , and the angles are between the incident and scattered rays and the normal to the mean surface plane. This solution was first published for acoustic waves in 1953,<sup>41</sup> and slightly later for electromagnetic scalar waves.<sup>42</sup>

The diffuse field solution is often expressed as a power expansion in both  $g$  and  $\lambda_o$ , the surface height correlation length. Interpretation of this solution requires assumptions about the surface roughness and its correlation function. For very rough, but Gaussian, surfaces ( $g \gg 1$ ), with a correlation function that is also Gaussian, the solution is:<sup>43</sup>

$$\langle I \rangle = \frac{k^2 F^2 \lambda_o^2 A_M}{4\pi r^2 g} \exp\left(-\frac{\lambda_o^2 (A^2 + B^2)}{4\sigma^2 C^2}\right) \quad (11)$$

where  $r$  is the distance from the scattering surface (assumed to be large), and the angular factors  $A$ ,  $B$ ,  $C$ , and  $F$  are given by:

$$A = \sin\theta_1 - \sin\theta_2 \cos\theta_3$$

$$B = -\sin\theta_2 \sin\theta_3$$

$$C = -(\cos\theta_1 + \cos\theta_2)$$

$$F = \frac{1 + \cos\theta_1 \cos\theta_2 - \sin\theta_1 \sin\theta_2 \cos\theta_3}{\cos\theta_1 + \cos\theta_2}$$

The first two angles, as previously stated, are respectively between the incident and scattered rays and the normal to the mean surface plane. The third angle,  $\theta_3$ , is between the normal planes containing incident and scattered rays, easily visualized as the angle between projections of incident and scattered rays into the mean surface plane.

For an exponential correlation function the average intensity is given instead by:<sup>44</sup>

$$\langle I \rangle = \frac{k^2 F^2 A_M}{4\pi r^2} \frac{g/\lambda_o}{[(g/\lambda_o)^2 + k^2 (A^2 + B^2)]^{3/2}} \quad (16)$$

This has the unphysical property of vanishing in the short wavelength (geometrical optics) limit due to the expansion of the exponential correlation function about the origin where the gradient is discontinuous.<sup>45</sup>

Although much more complicated, the same general assumptions of Kirchhoff analysis have been applied to vector waves appropriate for electromagnetism. However, the problem in using either scalar or vector results for ion beam textured metals is contained in some of these assumptions. Assumptions causing no problems include:

- The Kirchhoff approximation is valid ( $R$  must be constant or slowly varying).
- Observation is in the far field.
- Surface dimensions are larger than both incident wavelength and correlation length.
- Incident wave is planar and monochromatic.
- Surface statistics are isotropic.

Problematic assumptions directly affecting textured metals are:

- Multiple scattering is neglected, so there is no possibility for photon localization or depolarization.
- Shadowing and diffraction around features are neglected.
- All points on the surface are regular (differentiable). Fractal surfaces instead have infinite area and undefined gradients.

Formalisms have been identified that treat each of the three problematic assumptions with the possibility of eventual exact predictions for ion beam textures. The main effects of multiple scattering are increased depolarization and absorption.<sup>46</sup> Shadowing<sup>47</sup> and fractal<sup>48</sup> (diffractal scattering) effects primarily expand and deepen the absorption band, exactly the effects needed to account for the properties of ion textured baffle materials. Shadowing increases dramatically at oblique angles as illustrated in Figure 5. Fractal scattering is completely diffuse with coherent scattering strongly depressed.

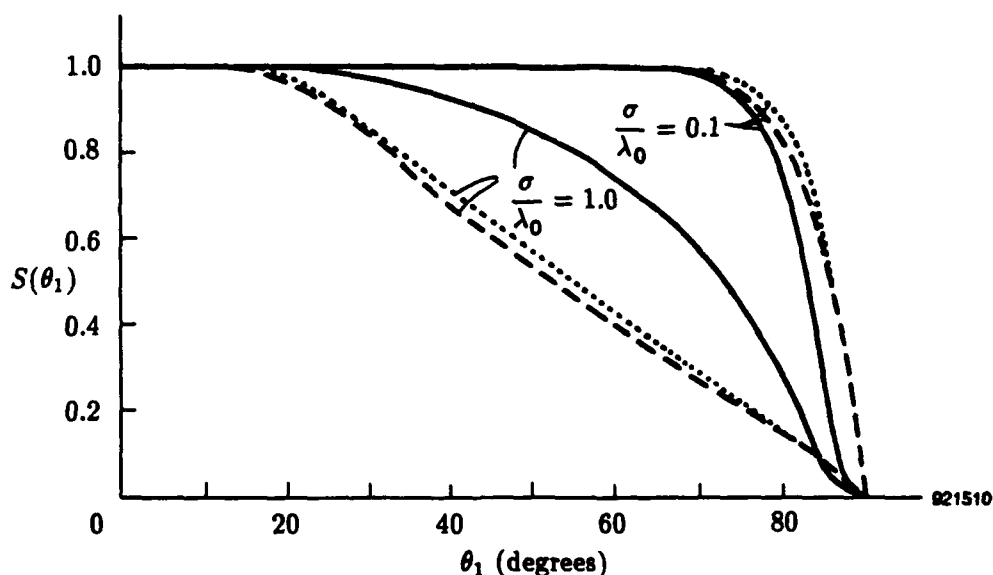


**Figure 5** Shadowing functions (multiplier) calculated by various authors (1965-69) for two ratios of rms height to correlation length.

The implication of these various formalisms for thermal emission, is that Kirchhoff analysis is close enough to predict general performance, while the effects of the problematic processes seem to account for the enhancement of the desired absorption band. Consequently, feature sizes should be adjusted to center the strongest Kirchhoff predicted optical absorption (at  $\lambda/2\pi$ ) near the peak of the Planck curve (or slightly on the long wavelength side) for the desired operating condition. Several scales of feature size, localization, and shadowing then broaden the absorption, but this is less critical than tuning to the required conditions, because the band is already broad enough to encompass most of the emission curve. This also implies that a textured refractory metal will be sufficient as a thermal emitter without an additional coating or blackening layer.

### 2.3 How Ion Beams Form Micro-Texture

The current model for explaining how seeding a foreign metal onto a surface during ion beam sputtering causes texture to form was developed in the mid-1970s by workers at NASA (Lewis).<sup>49</sup> Their measurements and tests supported a model in which atoms of seed material diffuse on the surface to congeal into protective islands as illustrated in Figure 6. The seed material intrinsically sputters more slowly than the substrate. This differential sputtering roughens the surface into characteristic features which evolve under further sputtering into the observed cones, spires, and rills.

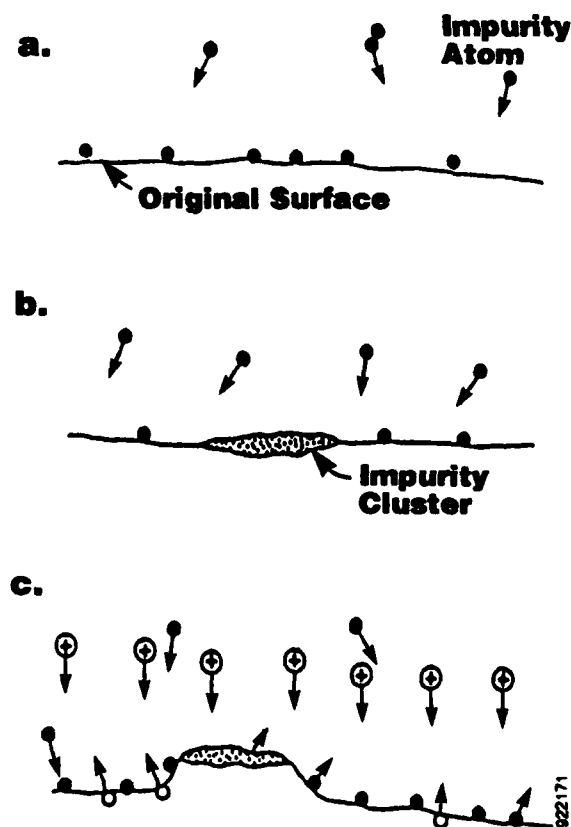


**Figure 6** *Microtexture is caused by differential sputtering between substrate and protective islands formed by seed material agglomerating on the surface.*

The problem with this diffusion model is that it strictly implies a correlation between feature size and diffusion rates which in turn depend on seed material properties, such as melting point. With a more extensive data base, we have found no correlation between feature size and any seed material property except heat of formation of the seed oxide. This implies that chemistry plays a strong role in feature formation and that residual vacuum chamber gases, particularly oxygen, may be critical. It should be noted that, in general, the oxides of a particular metal sputter much more slowly than the metal itself.

We are currently working to develop a more reliable model that incorporates oxide heat of formation. The first step is to accurately model the sputtering rate as a function of incident angle. The angular sputtering rate is responsible for propagation of surface gradients (features) once they are formed. Collisions of these propagating gradient fronts are at least partly responsible for the shape and distribution of features. Consequently, both the mechanism for initiation by seed material and later shape development by sputtering must be studied.

The best available theory on this subject is a linear cascade model developed by Sigmund in 1969.<sup>50</sup> Each incident ion shares kinetic energy with resting surface atoms in a series of binary collisions. The result is a cascade of fast recoils, which in turn set other target atoms in motion. As the number of affected atoms increases, their speed becomes progressively lower until, after a few times  $10^{-13}$  seconds, the edge collisions produce recoil energies below the threshold for atomic displacement, typically a few tens of eV. The agitated zone occupied by recoils in secondary and tertiary collisions is quenched by phonon-mediated energy dissipation after about  $10^{-9}$  seconds.

The sputter yield as a function of angle and incident energy is given by:

$$Y(E_i, \theta_i) = \frac{K_u}{U_o} S_n\left(\frac{E_i}{E_u}\right) f(\theta_i) \quad (17)$$

where  $S_n(E_i/E_u)$  is the reduced nuclear stopping cross section approximated by:

$$S_n(e) = 0.5 \frac{\ln(1 + e)}{[e + (e/383)^3/8]} \quad (18)$$

and the two scaling constants are:

$$E_u = (1/32.5) \left(1 + \frac{M_i}{M_t}\right) Z_i Z_t (Z_i^{2/3} + Z_t^{2/3})^{1/2} \text{ (keV)} \quad (19)$$

$$K_u = \frac{1}{3} (Z_i Z_t)^{5/6} \quad (20)$$

Note that all of the angular dependence is contained in the "angle-of-incidence" function  $f(\theta)$  which has been found to be approximated by:

$$f(\theta_i) = \cos^{-n} \theta_i, \quad \frac{2}{3} < n < \frac{5}{3} \quad (21)$$

Figure 7 shows the Sigmund prediction for sputtering rate as a function of incident angle for 1 keV argon on aluminum, the conditions used in this program for texturing aluminum. A similar curve applies to copper. The maximum sputtering rate angle becomes a preferred inclination for features. Since this angle causes maximum sputtering, surfaces at this angle propagate faster than others tending to erase them as features evolve into cones with identical aspect angles.

Thus, feature size (width or height) depends directly on how long a cone is protected by its seed island, which may in fact be an oxide island. The primary process parameter affecting this seems to be substrate temperature during sputtering, allowing a large range of feature sizes for a particular combination of seed and substrate materials. Feature density, in contrast, seems to depend on the ratio of seed atoms to beam atoms arriving at the surface.

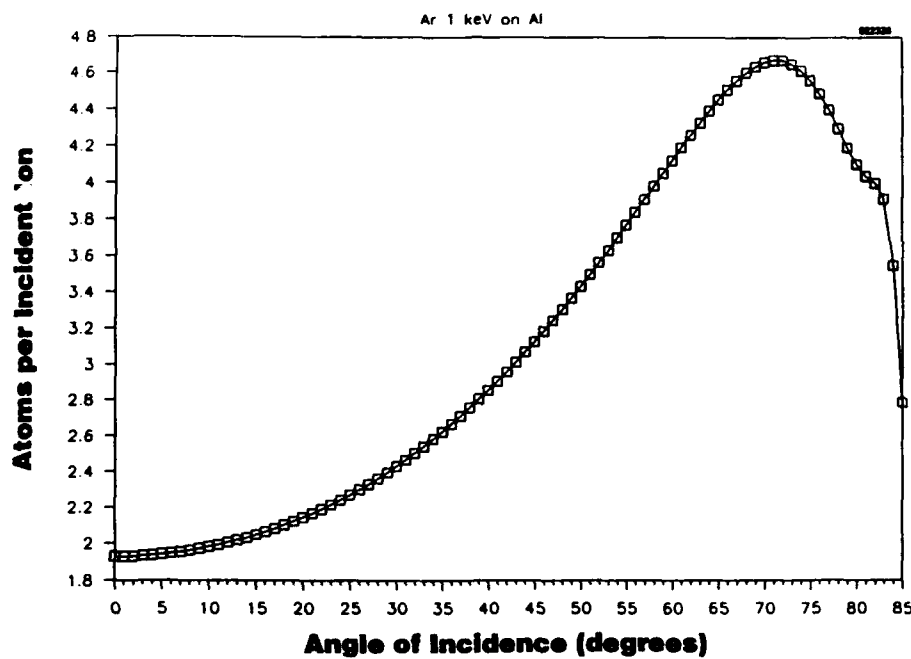


**Figure 7** *Sigmund model prediction of sputtering rate as a function of incidence angle for 1 keV argon ions bombarding aluminum.*

At the higher incident angles, not only does sputtering rate decrease, but more elastic grazing-angle scattering increases. Thus, when incident argon ions strike the steep sides of surface features, they tend to bounce and strike the surface again near the base of the feature, causing it to develop a "mote" around its base. Of course, these may not last long if sputtering continues and old features are erased as new ones form at their bases.

#### 2.4 Application to Heat Transfer

The objective of this project was to determine whether ion beam micro-texturing would enhance heat transfer through a surface under a variety of conditions. Two primary mechanisms were hypothesized to make this possible. First, broadband optical absorption promised to enhance thermal emission in purely radiative (high temperature) conditions. This was evaluated by measuring the absorption spectrum to determine how closely textured metal approximated an ideal blackbody. Radiative enhancement has also been tested by NASA's Lewis Research Center also using FTIR spectrometry in reflection mode.<sup>51,52</sup> A typical space radiator application is shown in Figure 8.

Secondly, micro-texturing was expected to increase surface area and thus directly contribute to conduction and convection, as do fins. The many small cavities were also expected to enhance nucleate boiling by reducing the excess temperature needed for nucleating bubbles to grow rather than collapse. In fact, the observed improvements in convection and nucleate boiling heat transfer are more likely due to improved wettability, which is known to help both.<sup>53-55</sup> In convective flows, better wetting decreases the boundary layer for laminar flow and disperses heat more effectively into the stream. In nucleate boiling, it causes bubbles to form with more fluid contact rather than vapor, again enhancing the net transfer coefficient. This is illustrated in Figure 9.

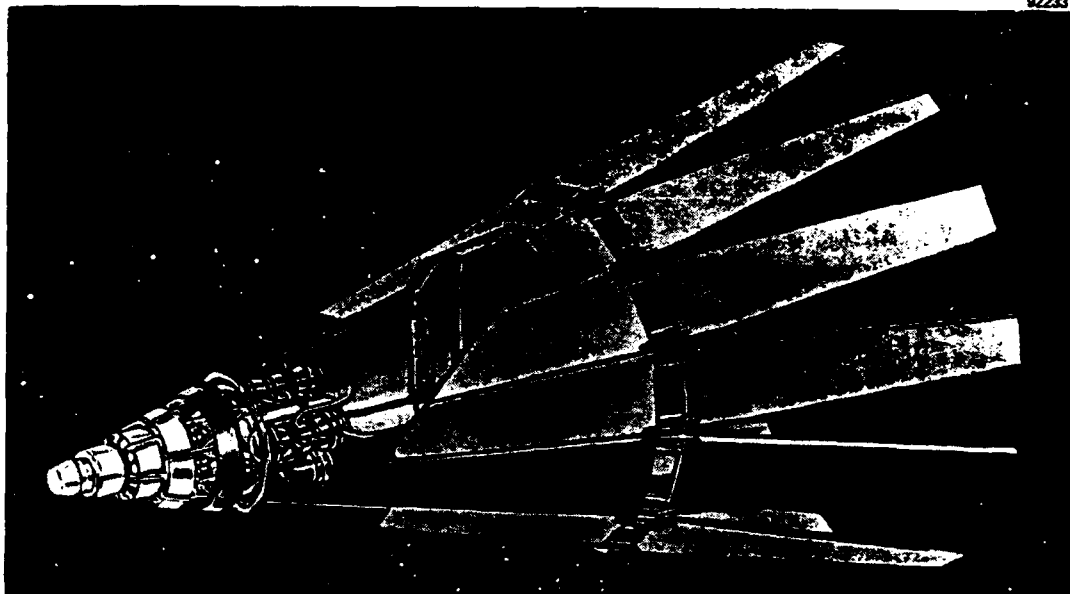


**Figure 8** *Typical space radiator application (SP 100 concept from reference 52).*

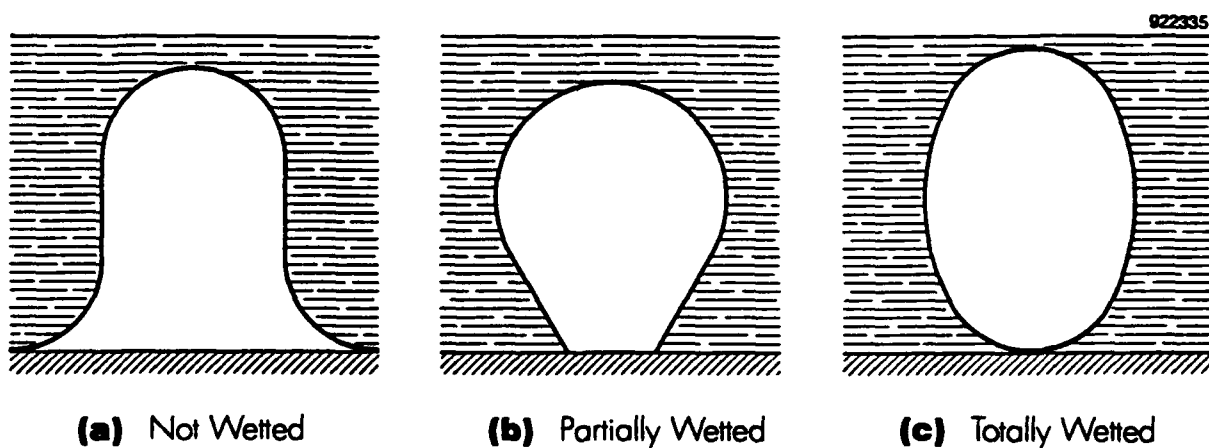


**Figure 9** *Effect of surface wettability on bubble contact angle.*

Contact angle measurements with water on samples of ion textured copper (but not aluminum) show dramatic changes in surface energy with texture; the contact angle nearly vanishes. Surfaces that have only been ion implanted, but not textured, also decrease contact angle, but it is a more modest decrease, typically about  $20^\circ$ . These effects, of implantation and texturing, seem to be additive but in this project were only measured with water and not refrigerants.

The hypothesized impact of surface area is suspect, because the feature sizes are so small ( $< 1 \mu\text{m}$ ), well below the dimensions of the boundary layer for any flow tested. They are even smaller than the wavelength of the phonons mediating conduction. Consequently, the effective surface area in all cases is the same as an untextured sample. This explains why there is no observable enhancement for conduction (still fluid) but some improvement when there is forced flow which compresses the boundary layer. Faster flows would therefore be expected to show an even greater effect.



### SECTION 3 EXPERIMENTAL PROCEDURE

For this project both copper and aluminum (6061-T6) samples were seeded by tantalum, although other seed materials are feasible. Historically, tantalum has been one of the best performers and the most thoroughly characterized. Argon ions were directed through a tantalum mesh causing some sputtering of tantalum onto the sample in addition to the rest of the argon flux. Thus, the surface was simultaneously seeded with tantalum and sputtered by argon.

An ion beam system (Figure 10) was used to treat flat circular 40 mm diameter coupons (coin-shaped) with a flat tantalum mesh. The aluminum samples were pre-heated to 480°F and irradiated for four hours at that temperature. Similar copper disks were heated to 450°F and treated for six hours. In both cases a mask around the edges created an untreated border about 3 mm wide.

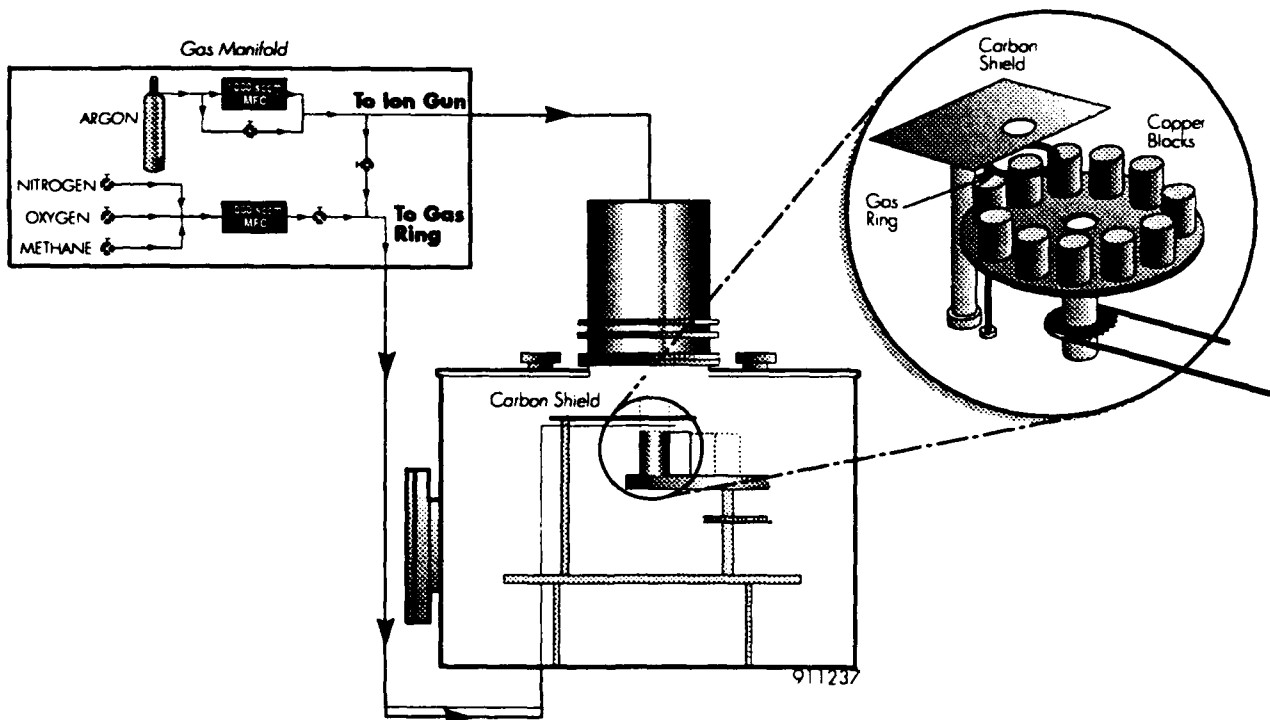


**Figure 10** *Ion beam texturing facility.*

For the pool-boiling experiment, a concentric cylinder of tantalum mesh surrounded the copper cylinder with about 10 mm of spacing between the two. The copper cylinder in turn jacketed a heater element. The copper cylinder was 25 mm in diameter and just over 100 mm

long. Both the copper and the concentric tantalum mesh were biased at -1,000 V while immersed in an ECR generated argon plasma as shown in Figure 11. As with the flat samples, roughly 1 keV argon atoms were thus directed through the mesh causing a small admixture of tantalum and argon to simultaneously reach the copper surface.

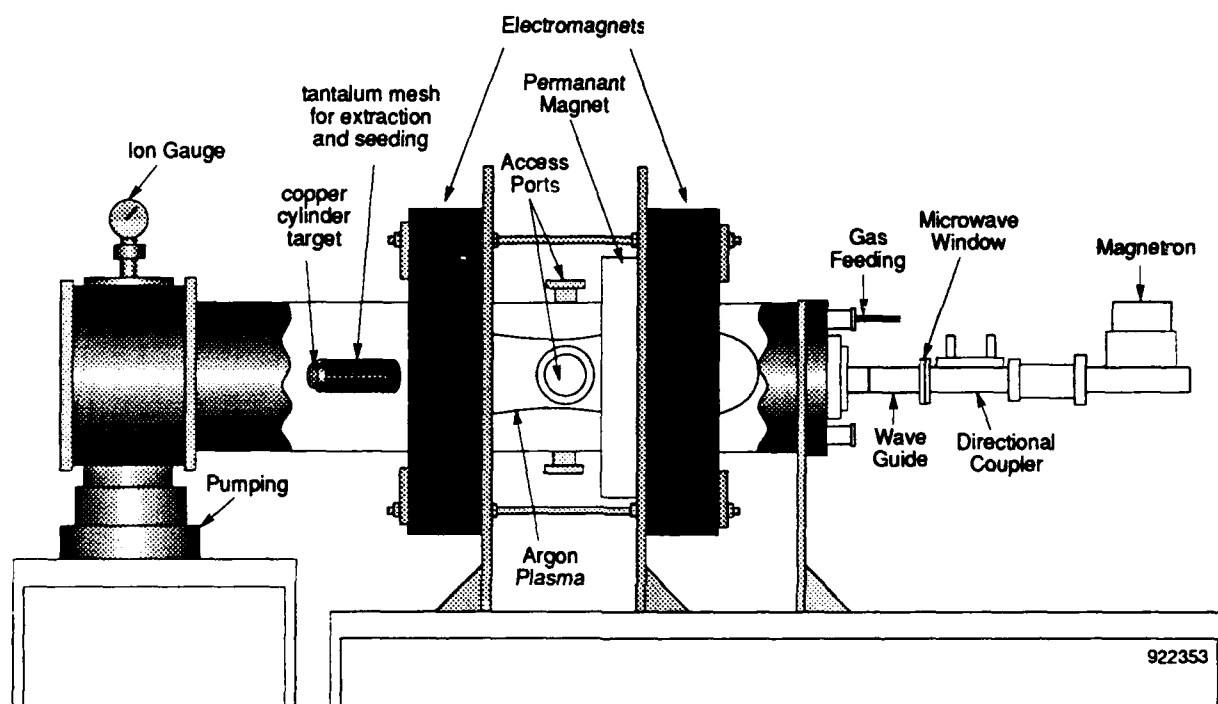


**Figure 11** *Plasma immersion texturing in an Electron Cyclotron Resonance (ECR) chamber.*

Heating during texturing caused the heater element inside the copper tube to detach. Apparently, a low melting point solder had been used for the original installation. This did not cause any problem, since the element was easily re-attached, and the surface texture is quite rugged, resisting damage from normal handling.

After treatment all samples were visibly darkened, but the cylinder was not uniform due to distortions in the mesh and an overlapping seam. Representative SEM views were taken, and optical properties were only measured for one sample of each material. This included Bidirectional Reflectance Distribution Function (BRDF, Breault Research Organization FASCAT scatterometer) and Fourier Transform Infrared Spectroscopy (FTIR, Nicolet Instruments/IBM) reflectivities. Reflectivity for each resulting grade of darkening allowed a deduction of thermal emissivity. Wettability was evaluated by measuring water contact angle in a shadow projection optical comparator (Gagemaster Series Twenty, Anaheim).

Two sets of textured and untreated metals, one set aluminum and one copper, were sent to Wright Laboratory (Dr. Won Chang) for incorporation into ongoing tests with heat pipes. To accommodate both ends of the pipeheat, a pair of disks was provided for each material condition. One sample of each material was also tested in a simple calorimetry rig to determine non-boiling heat flow characteristics. The larger copper cylinder was sent to the Rensselaer Polytechnic Institute Department of Mechanical Engineering (Dr. Michael Jensen) for tests of pool boiling in R-113 refrigerant.

The calorimetry rig consisted of a foam insulated beaker containing one liter of de-ionized water initially slightly below room temperature. The metal test disk was clamped by small screws to a round brass plate supported on an insulating polymer rod that suspended the disk horizontally touching the surface of the water as shown in Figure 12. A smaller metal cup holding about 100 ml of water sat on top of the brass plate with good thermal contact between them. The same configuration was used for each disk to prevent variations in geometry from affecting the basic heat flow.

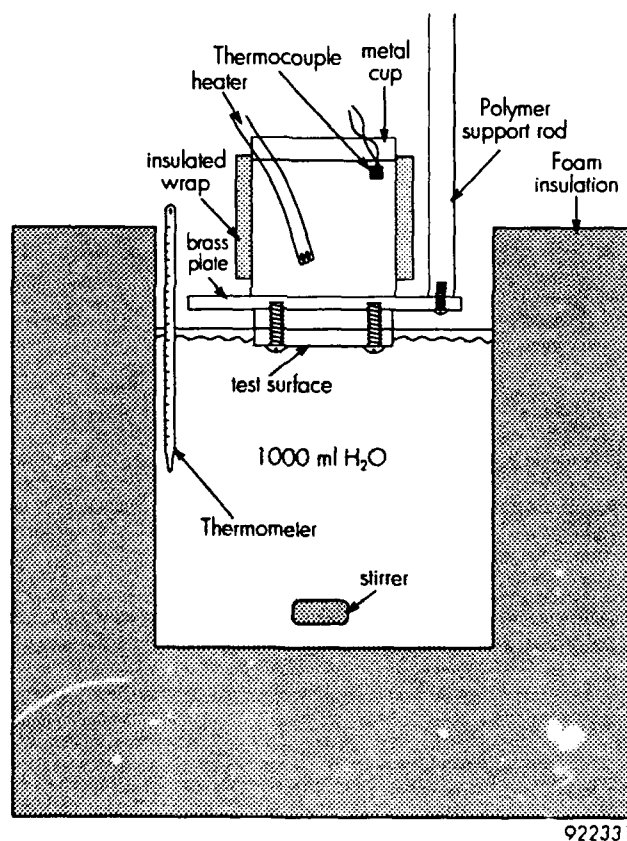


**Figure 12** *Calorimeter scheme for fluid transfer tests.*

A heater and thermocouple probe in the metal cup were powered to maintain a temperature of 80°C in the cup. A standard glass thermometer monitored temperature at the bottom of the large beaker. Measurements consisted of timing the interval for the large beaker to heat from 20 to 25°C. A similar measurement was made with a magnetic stirrer in the beaker to keep the fluid mixed as it warmed.

## SECTION 4 RESULTS

Only the visibly darkest aluminum was used for heat flow testing. The copper was quite black, but shiny flecks were also visible. Previous tests with copper had produced variable results depending on crystal orientation. The shiny areas again seem to be crystal faces with low feature concentrations. These are not evident in the SEM views shown in Figure 13, but there is some variability in concentration across the area examined. The corresponding SEM micrographs for aluminum, shown in Figure 14, also do not show any crystal orientations in the texture.

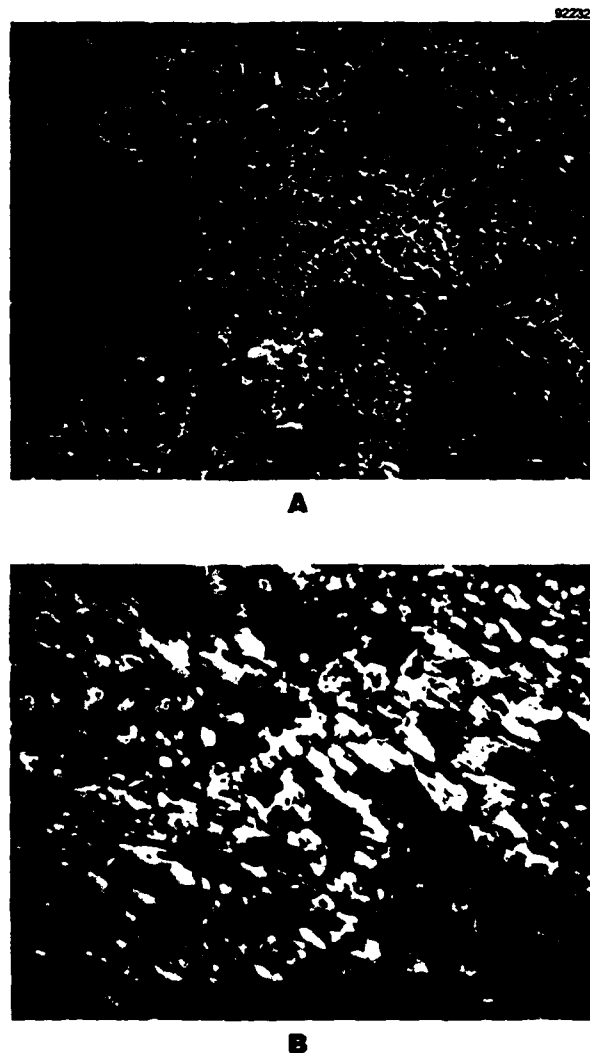


**Figure 13** *1,000X and 5,000X SEM micrographs of ion beam textured copper disk produced by six hours of argon bombardment at 1 keV through a tantalum mesh at a temperature of 450°F.*

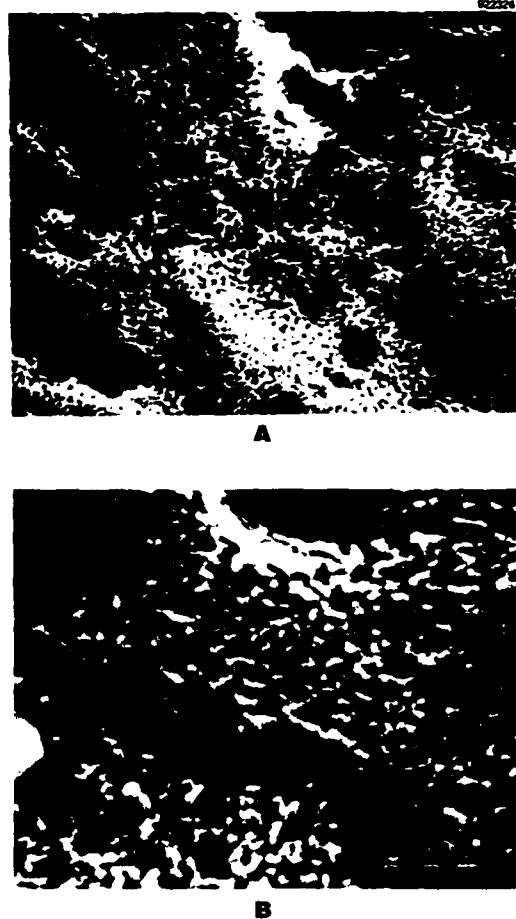


**Figure 14** *2,000X and 5,000X SEM micrographs of ion beam textured aluminum disk produced by four hours of argon bombardment at 1 keV through a tantalum mesh at a temperature of 480°F.*

Optical measurements, shown in Figures 15-18, indicate that both the aluminum and copper would be much more emissive than bare metal, better than 0.95 over the selected range of wavelengths of 2 to 25  $\mu\text{m}$ . Spectral emittance,  $\epsilon_\lambda$ , is derived from the FTIR reflectance measurements from:

$$\epsilon_\lambda = 1 - r_\lambda$$

where  $r_\lambda$  is the measured reflectance. This follows from conservation of energy and Kirchhoff's law applied to an opaque surface. Normal emittance for polish copper and aluminum is about 0.04. Other typical emittance values are shown in Figure 19.

Ideally these measurements should be performed at elevated temperatures to insure that the surface does not change due to chemical reactions or expansion. However, this was not possible in the limited scope of this project. Similar results for stainless steel and Ti6Al4V were obtained at elevated temperatures in a hohlraum reflectometer by NASA Lewis, as previously cited.<sup>51</sup> Together these results do prove, however, that texturing of more refractive metals would be useful in creating thermal radiators. Previous research has developed techniques for varying feature size and spacing to arbitrarily adjust the absorption band. Thus, ideal matches with the Planck emission curve can be obtained for a given temperature regime.

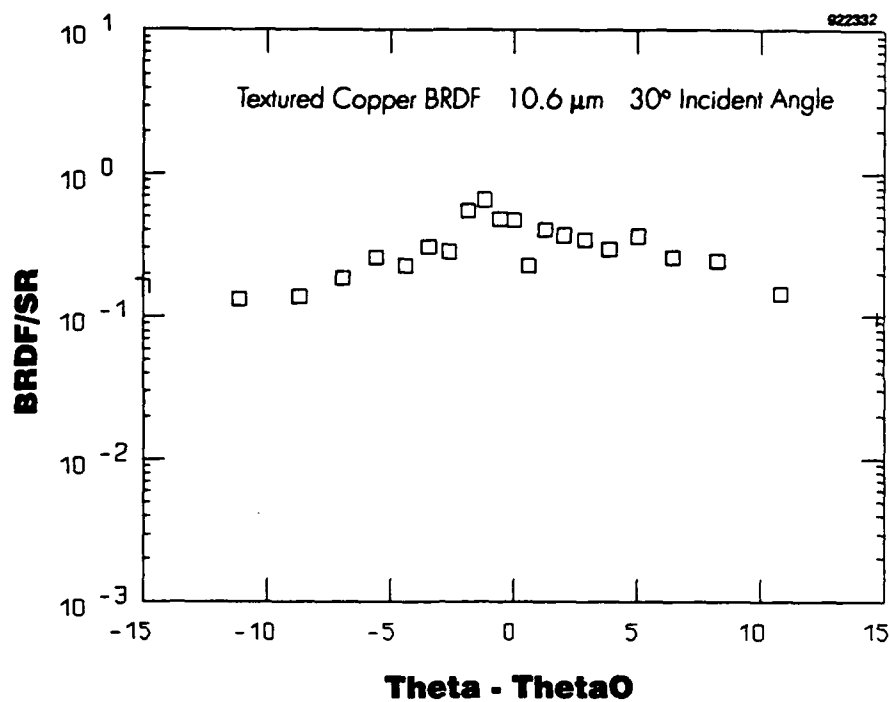


Figure 15 *BRDF for textured copper disk.*

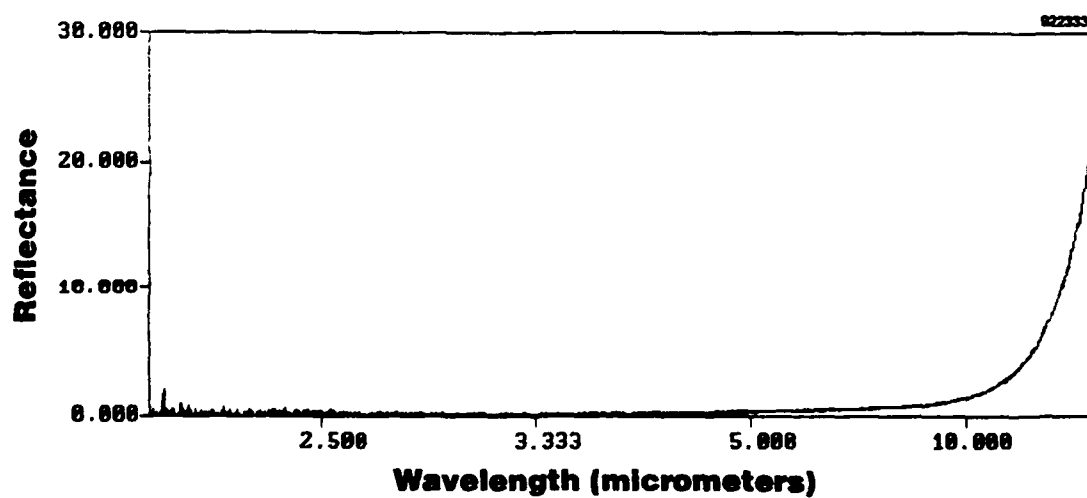


Figure 16 *FTIR reflectivity for textured copper disk.*

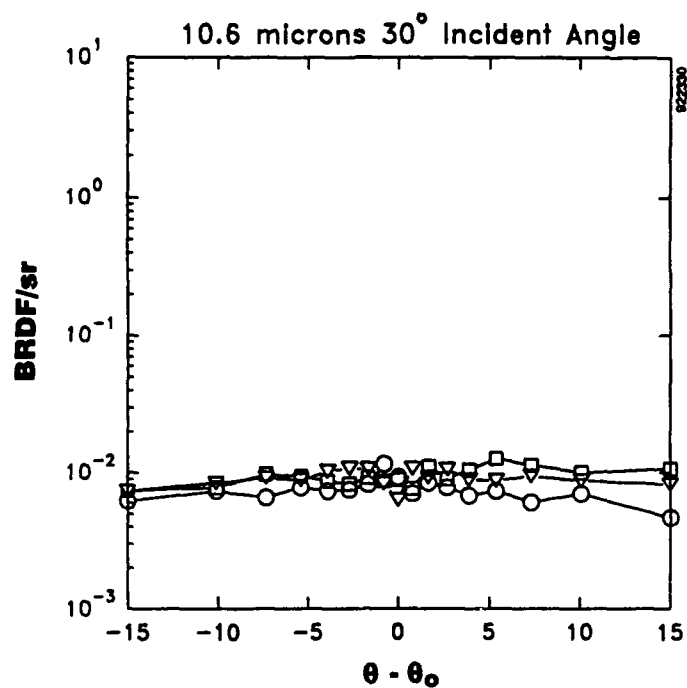


Figure 17 BRDF for three textured aluminum disks.

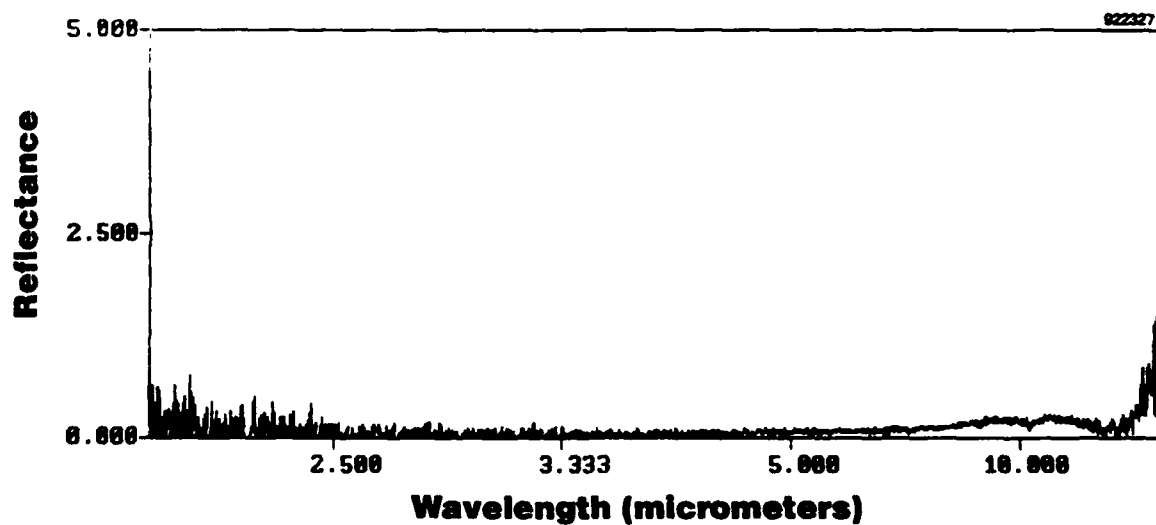
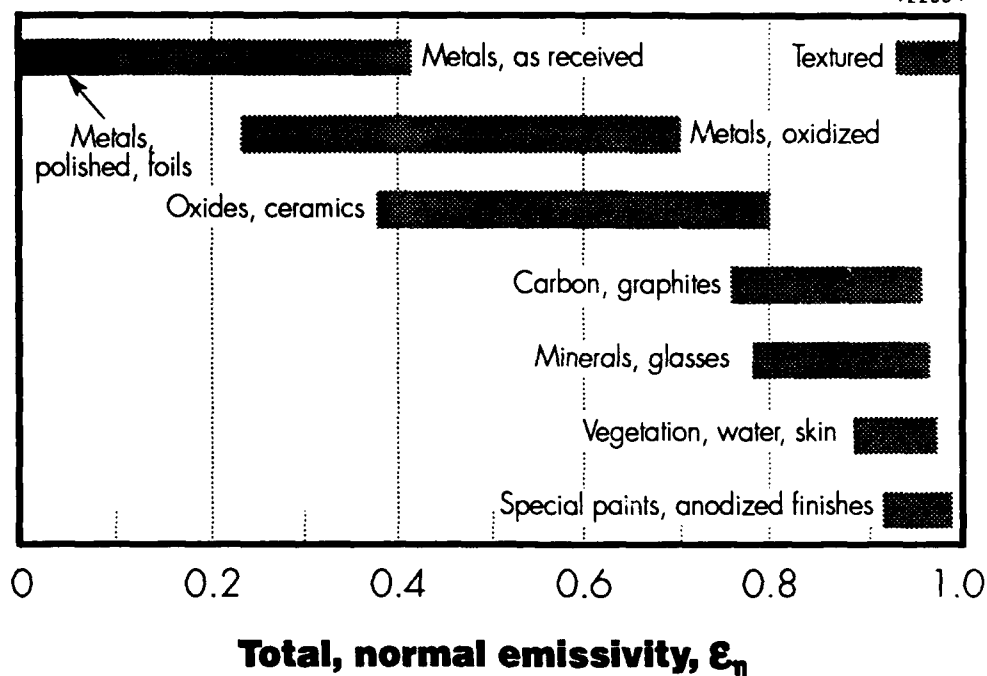


Figure 18 FTIR reflectivity for textured aluminum disk.



**Figure 19** *Representative values of total, normal emissivity.*

Wettability of several textured and ion implanted metals is indicated in Table I by the water contact angle measured in an optical comparator using medical grade HPLC water. In general, bare metals have relatively consistent wetting angles between 75 and 90°. Ion implantation reduces the wetting angle by 18 to 28°, making metal surfaces more hydrophilic. For copper, texturing reduces the contact angle to less than 4°, causing a water droplet to spread easily over a large area. This dramatic reduction of up to 85° certainly affects forced convection and nucleate boiling and may be entirely responsible for the observed enhancements of heat transfer under these conditions. Textured aluminum does not show a similar reduction, possibly because of a difference in feature sizes.

**Table I** *Effect of ion implantation and texture on selected materials.*

Material	Bare Metal	Ion Implanted	Textured
Co-Cr small radius curve	79.9	53.4	
Co-Cr moderate curve	79.0	61.4	
Co-Cr flat	78.8	51.3	
Ti-6Al-4V flat	67.6	51.5	5.0
Cu flat	89.0	43	3.7
Al flat	85	80	80



The pool boiling tests were conducted at the Rensselaer Polytechnic Institute's Department of Mechanical Engineering by Professor Michael Jensen who supplied the copper tube for texturing in the ECR plasma. Results comparing a partially textured tube with an untreated copy are shown in Figure 20. Although the increase in heat flux is relatively small for the average over the entire tube, it was estimated to reach as much as 50% for the textured area at 24,000 W/m<sup>2</sup>. A similar comparison to smooth metal for two commercially available surface structures is shown in Figure 21. Drawings of the types of structures involved are shown in Figure 22.

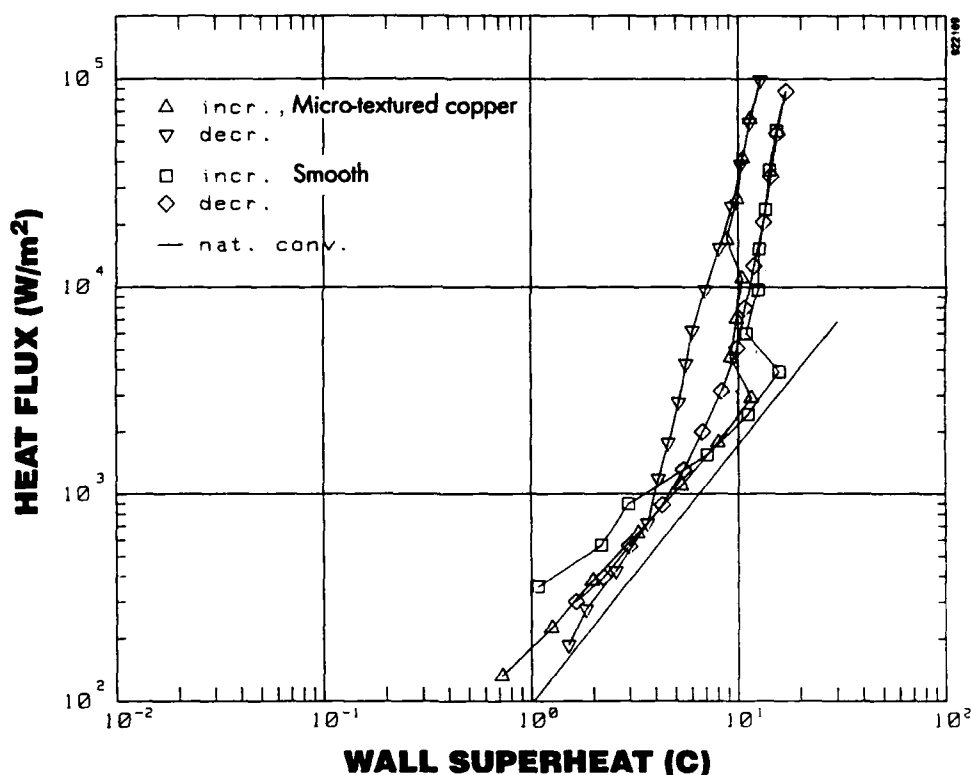


**Figure 20** *Pool boiling experiment comparing ion beam textured copper with bare metal and natural convection.*

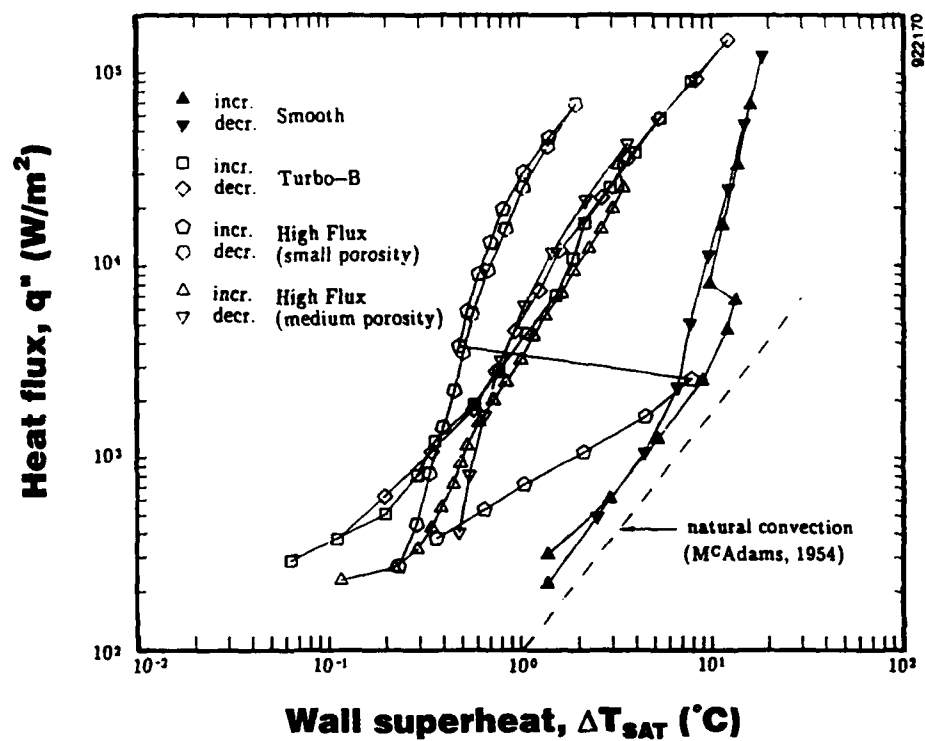
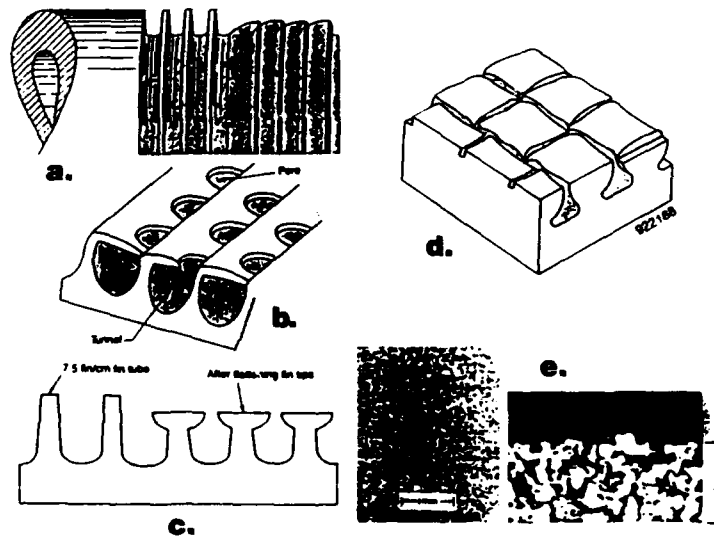


Figure 21 Pool boiling experiment comparing Turbo-B and two versions of High Flux structure in copper with bare metal and natural convection.



**Enhanced boiling surfaces**

- a. Rolled-over low fins
- b. Tunnel-and-pore arrangement
- c. Knurled low fins
- e. Sintered porous metallic matrix surface

Figure 22 Schematic drawings of commercially available structures advertised to enhance the heat transfer coefficient during nucleate boiling by up to a factor of 10.

It should be noted that the commercial structures have had many years of testing in which to optimize performance. Although the micro-textured metal caused a much smaller enhancement, this is still very promising for a first trial. It is particularly significant that nucleation clearly began in the textured areas at about  $\frac{1}{4}$  the heat flux of the untreated metal. Two approaches are likely to improve performance and eventually exceed that of available products. First, adjustments of feature size and density should be tested to find an optimal combination for heat transfer coefficient. The large change in surface wettability seems to correlate with enhanced nucleate boiling, so this parameter should be pursued to maximize heat transfer.

Secondly, the advantages of micro-texture (larger transfer coefficient and lower flux nucleation) could be combined with the macroscopic structures of available materials (Turbo-B or High Flux). Fins, tunnels, and other surfaces could be micro-textured prior to final shaping to create a composite structure with better nucleate boiling properties than either approach alone.

Calorimeter results were less promising than the nucleate boiling tests. As shown in Table II, texturing only showed significant improvement in heat transfer for copper with active flow. This is consistent with wettability changes shown in Table I, and does not support the hypothesized increase in effective surface area.

**Table II**      *Average time to change one liter of water from 20 to 25°C through a 40 mm diameter metal sample held at 80°C, in minutes with three trials for each condition.*

Sample	Not stirred	Stirred
Al - plain	11.7 +/- 0.2	8.5 +/- 0.4
Al - textured	11.8 +/- 0.2	8.4 +/- 0.6
Cu - plain	11.3 +/- 0.2	8.0 +/- 0.3
Cu - textured	11.2 +/- 0.3	7.2 +/- 0.4

## SECTION 5

### CONCLUSIONS AND RECOMMENDATIONS

#### 5.1 Conclusions

Phase I testing demonstrated that ion beam microtexturing of metal surfaces could be used to enhance heat transfer in three general configurations: (1) pure thermal emission, (2) convection to non-boiling fluids, and (3) nucleate boiling. The first one requires relatively high temperatures for the texture enhancement to be effective. Convection and nucleate boiling, however, can work at much lower temperatures using refrigerant fluids with low boiling points.

Originally developed at NASA's Lewis Research Center, ion beam texturing processes were refined by Spire to produce rugged broadband light absorbers, completely black from the visible to long wavelength IR. Therefore, they radiate more effectively, as well as increase the effective contact surface area for fluids. At higher temperature ranges, enhanced radiation adds significantly to total heat transferred.

Although the 50% enhancement of nucleate boiling is quite modest in comparison with commercially available systems, which promise up to a factor of ten enhancement over bare metal, this was only a first attempt. These other approaches have had many years to optimize performance, and micro-texturing could similarly improve. This potential in performance combined with the quite moderate cost of ion beam texturing strongly support the conclusion of feasibility.

#### 5.2 Recommendations

For pure thermal radiation applications, ion beam texturing could be quickly optimized by adjusting the absorption spectrum to match the required emission curve at the desired operating temperature. This can be achieved by changing feature size and density through control of the substrate temperature and beam currents during texturing. The center of the absorption band seems to depend mostly on feature size, while its width varies with feature spacing and other characteristics. For each combination of substrate material and beam species, feature size depends primarily on temperature during the process. Feature density is mostly a function of the ratio of substrate sputtering rate to seed material arrival rate. Thus, the size and position of the absorption (emission) band can be directly controlled.

In addition, sputtering conditions can be varied during the process to create a distribution of feature sizes to further broaden absorption. This may also enhance convection and nucleate boiling and should not be restricted to sizes affecting visible and IR optical properties. Combinations of micro-texturing with larger structures should also be explored. In particular, hybrids of micro-texture with commercially available surfaces incorporating fins, macroscopic folds, and corrugation could multiply their respective enhancements to achieve much larger composite effects.

In addition to hypersonic airframes and scramjets calling for active cooling, many other advanced performance systems would benefit from this capability. Satellite power systems, micro-electronics, electric aircraft, engines, transformers, generators, and motors could all perform better with enhanced heat removal. Heat pipes, capillaries, and higher temperature radiators would all perform better with micro-textured surfaces. Large components, or large batches of smaller components, for these systems should be treated by a large scaled-up process based on ECR plasma extraction rather than relatively low-current ion beams.

SECTION 6  
REFERENCES

1. A. Guenterschultze and W. Tollmien, *Z. Physik*, **119**, 685, (1942).
2. O. Auciello and R. Kelly, Ion Bombardment Modifications of Surfaces: Fundamentals and Applications, (1984).
3. B.A. Banks, "Ion Beam Applications Research- A 1981 Summary of Lewis Research Center Programs, NASA, TM, 81721, (1981).
4. W.R. Hudson (NASA-Lewis), "Ion Beam Texturing," *J. Vac. Sci. Technol.* **14**(No.1), 286-9 (1977).
5. O. Auciello, "Ion Interaction With Solids," and "Surface Texturing, Some Bulk Effects and Their Possible Applications," *J. Vac. Sci. Technol.* **19**(No. 4), (1981).
6. W.D. Deininger and S.B. Gabriel, "Mandrels for Microtextured Small-Vessel Implants," NASA Tech. Brief, **13**, No. 3, Item #142, (1989).
7. S.M. Rossnagel and R.S. Robinson, "Surface Diffusion Activation Energy Determination Using Ion Beam Micro-texturing," *J. Vac. Sci. Technol.* **20**(No. 2), 195-8 (1982).
8. C.J. Von Benken and E.A. Johnson, "Role of Impurities in the Growth of Surface Features Due to Ion Beam Bombardment," Unpublished, (1989).
9. L.L. Foldy, "The Multiple Scattering of Waves," *Phys. Rev.* **67**, 107-119 (1945).
10. M. Lax, "Multiple Scattering of Waves," *Rev. Mod. Phys.* **23**, 287 (1951).
11. M. Lax, "Multiple Scattering of Waves II. The Effective Field in Dense Systems," *Phys. Rev.* **85**, 621-629 (1952).
12. N.C. Mathur and K.C. Yeh, "Multiple Scattering of Electromagnetic Waves by Random Scatterers of Finite Size," *J. Math Phys.* **5**, 1619-1628 (1964).
13. V. Twersky, "Coherent Electromagnetic Waves in Pair-Correlated Random Distributions of Aligned Scatterers," *J. Math Phys.* **19**, 215-230 (1978).
14. K. M. Hong, "Multiple Scattering of electromagnetic Waves by a Crowded Monolayer of Spheres: Application to Migration Imaging Films," *J. Opt. Soc. Am.* **70**, 821-6 (1980).
15. M.A. Biot, *J. Appl. Phys* **28**, 1455 (1957).
16. M.A. Biot, *J. Appl. Phys* **29**, 998 (1958).
17. H. Davies, *Proc. Inst. Elec. Engrs. (London)* **101**, 209 (1954).
18. H.E. Bennett and J.O. Porteus, "Relation Between Surface Roughness and Specular Reflectance at Normal Incidence," *J. Opt. Soc. Am.* **51**, 123 (1961).
19. J.O. Porteus, "Relation Between the Height Distribution of a Rough Surface and the Reflectance at Normal Incidence," *J. Opt. Soc. Am.* **53**, 1394 (1963).
20. Philip M. Morse and K. Uno Ingard, *Theoretical Acoustics*, McGraw-Hill, New York, 1968.
21. N.F. Mott and E.A. Davis, *Electronic Processes in Non-crystalline Materials*, 2nd Ed., Clarendon Press, Oxford, 1979.
22. See, for an early example, R.D. Evans, *The Atomic Nucleus*, McGraw-Hill, NY, 1955 or R.G. Newton, *Scattering Theory of Waves and Particles*, McGraw-Hill, NY, 1966.
23. P.W. Anderson, *Phys. Rev.* **109**, 1492 (1958).
24. S. John, *Phys. Rev. Lett.* **53**, 2169 (1984).
25. P.W. Anderson, *Philos. Mag. B* **52**, 505 (1985).

26. K. Arya, Z.B. Su and J.L. Birman, "Anderson Localization of Electromagnetic Waves in a Dielectric Medium of Randomly Distributed Metal Particles," *Phys. Rev. Lett.* **57**, 2725 (1986).
27. S. John, "Strong Localization of Photons in Certain Disordered Dielectric Superlattices," *Phys. Rev. Lett.* **58**, 2486 (1987).
28. G.H. Watson, Jr., P.A. Fleury and S.L. McCall, "Search for Photon Localization in the Time Domain," *Phys. Rev. Lett.* **58**, 945 (1987).
29. J.D. Maynard, "Acoustical Analogs for Solving Condensed Matter Problems," *J. Acoust. Soc. Am.* **85**, 2226 (1989).
30. D. Sornette and B. Souillard, "Strong Localization of Waves by Internal Resonances," *Europhys. Lett.* **7**, 269 (1988).
31. Philip M. Morse and K. Uno, *Theoretical Acoustics*, McGraw-Hill, New York, 1968.
32. V. Twersky, *J. Opt. Soc. Am.* **52**, 145 (1962).
33. Louis Harris, "Optical Properties of Metal Blacks and Carbon Blacks," *Monograph Series No. 1*, Eppley Foundation for Research, Newport, RI, 1967.
34. Anton Greenwald, Unpublished Master's project, U. Maryland, 1971.
35. J.A. Greenwood and J.P.B. Williamson, "Developments in the Theory of Surface Roughness," *Surface Roughness Effects in Lubrication, Proc. 4th Leeds-Lyon Symp. on Tribology*, Lyon, Sep., 1977, D. Dowson, C.M. Taylor, M. Godet and D. Berthe, Eds., Mech. Eng. London, pp. 167-177, 1978.
36. T.R. Thomas, Ed., *Rough Surfaces*, Longman, New York, 1982.
37. D.J. Whitehouse and J.F. Archard, "Properties of Random Surface of Significance in Their Contact," *Proc. Roy. Soc.* **A316**, 97-121 (1970).
38. M. Rasigni and G. Rasigni, "Surface Structure Autocorrelation Functions and Their Fourier Transforms for Rough Deposits of Magnesium," *Phys. Rev.* **B19**, 1915-19 (1979).
39. S.M. Goodnick, D.K. Ferry, C.W. Wilmsen, Z. Liliental, D. Fathy and O.L. Krivanek, "Surface Roughness at the Si(100)-SiO<sub>2</sub> Interface," *Phys. Rev.* **B32**, 8171-85 (1985).
40. G.R. Kirchhoff, *Vorlesung uber Mathematische Physik Vol. II*, Teubner, Leipzig, 1891.
41. C. Eckart, "Scattering of Sound from the Sea Surface," *J. Acou. Soc. Am.* **25**, 556-570 (1953).
42. W.C. Ament, "Toward a Theory of Reflection by a Rough Surface," *Proc. IRE*, **41**, 142-146 (1953).
43. P. Beckman and A. Spizzichino, *The Scattering of Electromagnetic Waves from Rough Surfaces*, Pergamon, Oxford, 1963 (Reprinted by Artech House, Inc., Norwood, MA, 1987).
44. C.W. Horton and T.G. Muir, "Theoretical Studies on the Scattering of Acoustic Waves from a Rough Surface," *J. Acous. Soc.* **41**, 627-634 (1966).
45. D.E. Barrick, "Relationship between Slope Probability Density Function and the Physical Optics Integral in Rough Surface Scattering," *Proc. IEEE* **56**, 1728-29 (1968b).
46. M.A. Biot, "Generalized Boundary Conditions for Multiple Scatter in Acoustic Reflection," *J. Acous. Soc.* **44**, 1616-1622 (1968).
47. M.V. Berry, "DiffRACTals," *J. Phys. A: Math Gen.* **12**, 781-797 (1979).
48. M.I. Sancer, "Shadow-Corrected Electromagnetic Scattering from a Randomly Rough Surface," *IEEE Trans. Ant. Prop.* **AP-17**, 577-585 (1969).
49. S.M. Rossnagel and R.S. Robinson, "Monte Carlo Model of Topography Development During Sputtering," *J. Vac. Sci. Technol.* **A1**(2), 426 (1983).

50. P. Sigmund, *Phys. Rev.* **184**, 383(1969) and **187**, 768(1969).
51. M.J. Mirtich, F. DiFilippo, J. Barry, and M. Kussmaul, "Emittance of Space Radiator Materials Measured at Elevated Temperatures," 15th Intl. Conf. on Metallurgical Coatings, Am. Vac. Soc., San Diego, April, 1988, also NASA Tech. Memorandum 101948.
52. M.J. Mirtich and M. Kussmaul, "Enhanced Thermal Emittance of Space Radiators by Ion-Discharge Chamber Texturing," 14th Intl. Conf. on Metallurgical Coatings, Am. Vac. Soc., San Diego, March, 1987, also NASA Tech. Memorandum 100137.
53. Frank P. Incropera and David P. DeWitt, *Fundamentals of Heat Transfer*, John Wiley & Sons, NY, 1981.
54. Frank Kreith and William Z. Black, *Basic Heat Transfer*, Harper & Row, NY, 1980.
55. J.T. Davies and E.K. Rideal, *Interfacial Phenomena*, Academic Press, NY, 1961.